Lifetime measurement for the possible antimagnetic rotation band in ^{101}Pd

M. Sugawara*
Chiba Institute of Technology, Narashino, Chiba 275-0023, Japan

T. Hayakawa, M. Oshima, Y. Toh, A. Osa, M. Matsuda, T. Shizuma, and Y. Hatsukawa
Japan Atomic Energy Agency, Tokai, Ibaraki 319-1195, Japan

H. Kusakari
Chiba University, Inage-ku, Chiba 263-8522, Japan

T. Morikawa
Kyushu University, Hakozaki, Fukuoka 812-8581, Japan

Z. G. Gan
Institute of Modern Physics, Chinese Academy of Science, Lanzhou 730000, People's Republic of China

T. Czosnyka
Heavy Ion Laboratory, Warsaw PL-02097, Poland
(Received 16 May 2015; revised manuscript received 11 July 2015; published 10 August 2015)

Lifetime measurements were made for the $\nu h_{11/2}$ band in ^{101}Pd, which had been interpreted as a possible antimagnetic rotation band based on the comparison of $I-\omega$ behavior with the calculation of a semiclassical particle-rotor model in our previous study. Doppler broadened line shapes were analyzed for the decaying γ rays in the band following the reaction ^{68}Zn(^{37}Cl, 1p3n)^{101}Pd. The semiclassical particle-rotor model was modified to reproduce both the $I-\omega$ plot and the $B(E2)$ behavior simultaneously for the antimagnetic rotation bands in Pd and Cd nuclei, for which $B(E2)$ values had been measured so far. Reasonable agreements between the experiment and the calculation were obtained. It is concluded that the lower part of the $\nu h_{11/2}$ band in ^{101}Pd can be interpreted as an antimagnetic rotor.

DOI: 10.1103/PhysRevC.92.024309 PACS number(s): 21.10.Tg, 23.20.−g, 25.70.−z, 27.60.+j

I. INTRODUCTION

Magnetic rotation (MR) and antimagnetic rotation (AMR) are interesting nuclear structures observed around doubly magic nuclei. The MR band can be easily distinguished from the normal rotational band because it consists almost exclusively of $M1$ cascade transitions. However, the AMR band is subtle in this respect as it consists of stretched $E2$ transitions, which is similar to the normal rotational band. To prove the AMR character, it is required to show experimentally both large ratios of the dynamic moments of inertia $\mathrm{Im}^{(2)}$ to the reduced transition probability $B(E2)$ values and the decreasing behavior of $B(E2)$ with the increasing spin [1]. Therefore, lifetime measurements are crucial for claiming the AMR character for the proposed band.

Recently, several AMR bands have been confirmed in Pd and Cd nuclei around mass number $A = 100 \sim 110$ from the lifetime measurements with the Doppler shift attenuation method (DSAM) [2–7]. Relevant high-j orbitals for AMR in this region are $\pi g_{9/2}$ as a hole state and $\nu h_{11/2}$, $\nu g_{7/2}$, and $\nu d_{5/2}$ as particle states. One of the bands observed in ^{101}Pd was interpreted as a possible candidate for AMR based on the $I-\omega$ behavior in our previous study [8]. Because a thick target was used in that experiment, it is possible to extract lifetimes for the proposed band through the analysis of Doppler broadened line shapes of γ rays.

It is important to note here that, in some nuclei in this region, a so-called smoothly terminating band (STB) is observed [9]. Its structure resembles that of AMR in the sense that both are related to the alignment of angular momenta of valence nucleons around a weakly deformed core. In fact, $B(E2)$ value is small and decreases as spin value increases in both the cases. However, an important difference between STB and AMR is in the behavior of $\mathrm{Im}^{(2)}$ along the band. While it goes down according with $B(E2)$ value in STB, it is essentially constant reflecting shears mechanism in AMR. Consequently, one of the peculiar characters for AMR is the largeness and rise of $\mathrm{Im}^{(2)}/B(E2)$ values along the band [10].

The present study reports the lifetimes of the $\nu h_{11/2}$ band in ^{101}Pd newly determined through the analysis of the data in our previous experiment. It is found that the deduced $B(E2)$ values conclusively establish the AMR character of the band. This paper is organized as follows. First, we describe the experimental methods and results in Sec. II. The discussion in Sec. III includes the description of the $\nu h_{11/2}$ band on the basis of a semiclassical particle-rotor model modified to include neutron alignments while the shears are closing. The results of model calculations are compared with the experimental data in the same section. A summary is given in Sec. IV.

*masahiko.sugawara@it-chiba.ac.jp

II. EXPERIMENTAL METHODS AND RESULTS

The high spin states of ^{101}Pd were populated through the reaction ^{68}Zn(^{37}Cl, 1p3n)^{101}Pd. An enriched ^{68}Zn foil with a thickness of 10 mg/cm^2 was bombarded with a 125-MeV ^{37}Cl beam provided by the tandem accelerator at the Japan Atomic Energy Agency (JAEA). Gamma rays emitted from the excited states were detected with an array of 12 HPGe detectors with BGO Compton suppressors (GEMINI) [11]. The HPGe detectors were placed at angles of 32°, 58°, 90°, 122°, and 148° with respect to the beam direction. The details of the experiment were described in Ref. [8].

Because the target was thick enough for residuals to stop inside the target, lifetimes of the high spin states can be extracted from the Doppler broadened line shapes of the decaying γ rays. To obtain the angle dependent γ-ray line shapes, we sorted γ-γ coincidence events to three asymmetric matrices whose x axes were the γ-ray energies in the detector at 32° or 148°, 58° or 122°, and 90°, while the y axes for these matrices were the γ-ray energies in the detector at any position. The three angle-dependent γ-ray spectra obtained by setting a gate on the 670-keV transition from $\frac{11}{2}^-$ to $\frac{9}{2}^+$ were used for the lifetime analysis.

The observed γ-ray line shapes in the three angle-dependent spectra were simultaneously analyzed with the code LINESHAPE developed by Wells and Johnson [12]. A Monte Carlo simulation was done in time step of 0.0011 ps for 10 000 histories to generate a velocity profile of residuals in the target. A total of 10-mg/cm^2 thickness was divided into an effective target area of 2 mg/cm^2 and an effective stopper area of 8 mg/cm^2 taking account of energy losses of recoils in the target material. The stopping power was calculated according to the formula with shell correction of Northcliffe and Schilling [13].

The energies of the γ transitions in the band of interest and the side-feeding intensities were treated as the input parameters to the line-shape analysis. The side-feeding intensities were obtained from the spectrum for 90° detectors and fixed in the fitting procedure. The side-feeding into each level in the band was assumed as a rotational cascade of five transitions. The quadrupole moments of the side-feeding sequence, when combined with the moment of inertia, gave an appropriate effective side-feeding time for each level. The moment of inertia of $28\hbar^2$ MeV^{-1} was adopted as an averaged value over the neighboring nuclei. For each line-shape combination, the in-band and side-feeding quadrupole moments, the background parameters, and the intensities of contaminant peaks were allowed to vary. The χ^2 minimization routines of MINUT [14] were used to fit the simulated line shapes to the observed spectra.

The band of interest in the present analysis is the $\nu h_{11/2}$ band (band 3 in Ref. [8]) in ^{101}Pd which was claimed to be a possible candidate for AMR in our previous paper [8]. The cascade $E2$ transitions comprising the $\nu h_{11/2}$ band are shown in Fig. 1. First, the highest transition of 1494 keV [$(\frac{51}{2}^-)\rightarrow\frac{47}{2}^-$] was assumed to have 100% side-feed. The other parameters were allowed to vary until the least χ^2 value was attained. This provided us with the effective lifetime for the $(\frac{51}{2}^-)$ level. This effective lifetime was then used as the input parameter to deduce the side-feeding lifetime to and the lifetime of the next lower level in the band. The χ^2 minimization process for the individual level was repeated in this way until the lowest level of the band was reached. Finally, the lifetimes of all the states in the band were deduced from a global fit of the full cascade where only the in-band and side-feeding lifetimes were allowed to vary. The uncertainties in the lifetime measurements were obtained from the χ^2 behavior in the vicinity of the minimum for the simultaneous fit for the three angle-dependent spectra using the MINOS [14] routine. The other source of statistical error was the uncertainty in the sidefeeding intensity, which was estimated to be 5%. The final statistical uncertainty was calculated by adding the two uncertainties mentioned above in quadrature.

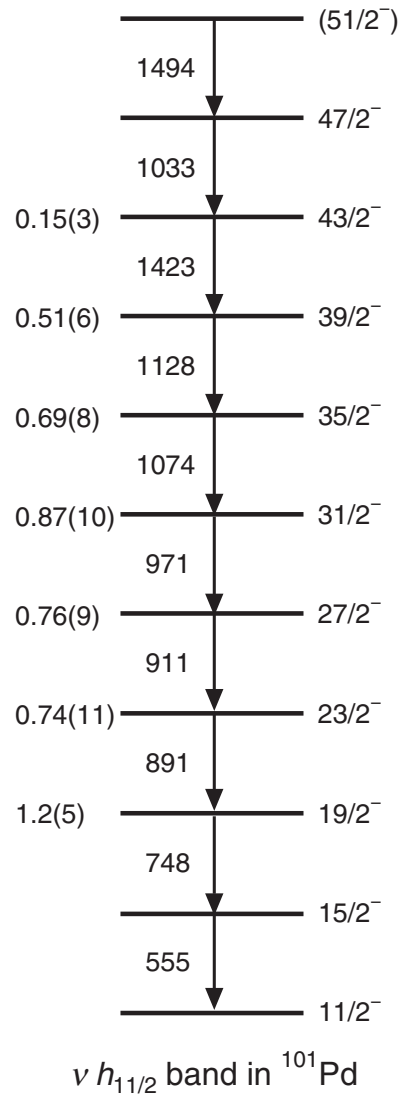

FIG. 1. The level scheme of the $\nu h_{11/2}$ band (band 3 in Ref. [8]) in ^{101}Pd. The energies of γ transitions are given in keV. On the left of each state are the deduced mean lives in picoseconds. Statistical uncertainties are shown in parentheses.

The mean lifetimes and statistical uncertainties obtained from the line-shape analysis are given in Fig. 1, where the values are not shown for the uppermost two levels. Those are treated just as input parameters to deduce the lifetimes for the

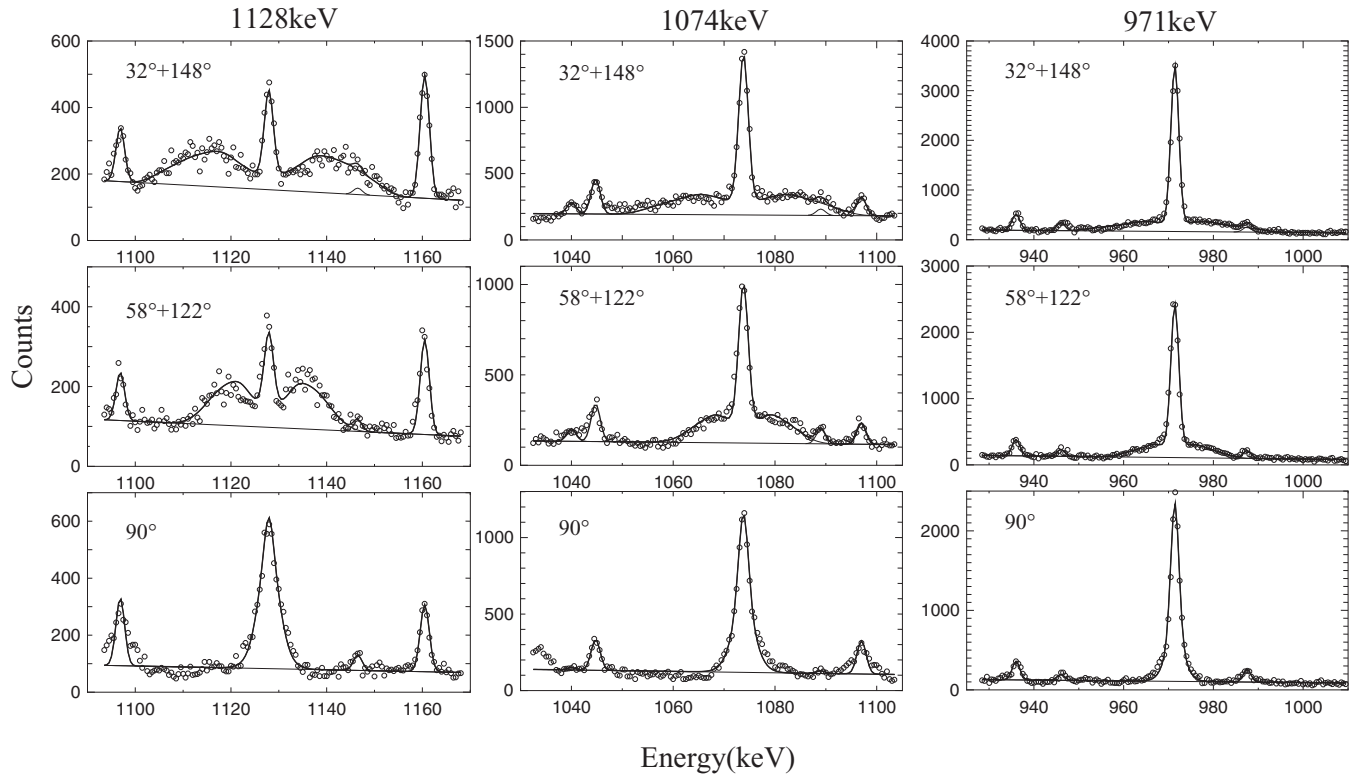

FIG. 2. Examples of the line-shape fits for 1128 keV ($\frac{39}{2}^- \rightarrow \frac{35}{2}^-$), 1074 keV ($\frac{35}{2}^- \rightarrow \frac{31}{2}^-$), and 971 keV ($\frac{31}{2}^- \rightarrow \frac{27}{2}^-$) transitions at 32° (or 148°), 58°(or 122°), and 90° with respect to the beam direction. The results of the fits to the experimental spectra are shown as thick lines while the contaminant peaks are shown as thin lines.

lower levels because the reliable values could not be obtained because of lower statistics and serious contaminant peaks. It should be noted that the quoted errors in the figure do not include additional systematic errors, which may be as large as 20% and stem from the choice of the stopping powers and the effective target thickness used in the analysis. Examples of the line-shape fits for the three cascades in the band are shown in Fig. 2. The deduced $B(E2)$ values and the ratios of $\mathrm{Im}^{(2)}$ to $B(E2)$ are tabulated in Table I which shows clearly the large $\mathrm{Im}^{(2)}/B(E2)$ values and the decreasing tendency of $B(E2)$ with the increasing spin at the lower part of the band. The relatively large error in the value for the $\frac{19}{2}^-$ level could be from low sensitivity of the line shape itself and correlation with the parameters for the higher levels.

TABLE I. The deduced $B(E2)$ values and the ratios of $\mathrm{Im}^{(2)}$ to $B(E2)$ for the cascade of the $\nu h_{11/2}$ band in ^{101}Pd. The corresponding statistical errors are given in parentheses.

Initial spin I_i $[\hbar]$	$B(E2)$ $[(\mathrm{eb})^2]$	$\mathrm{Im}^{(2)}/B(E2)$ $[\hbar^2\mathrm{MeV}^{-1}(\mathrm{eb})^{-2}]$
$19/2^-$	0.29(11)	98(39)
$23/2^-$	0.19(3)	1029(160)
$27/2^-$	0.17(2)	395(49)
$31/2^-$	0.105(12)	371(41)
$35/2^-$	0.082(9)	899(102)
$39/2^-$	0.087(10)	155(18)
$43/2^-$	0.09(2)	

III. DISCUSSION

We first compare the present $B(E2)$ values with those for neighboring Pd nuclei to examine whether the reasonable values were obtained or not in the present experiment. The experimental $B(E2)$ values which have been known so far are shown as functions of spin values for ^{100}Pd, ^{101}Pd, ^{102}Pd, and ^{104}Pd in Fig. 3. It is clear that the present $B(E2)$ values for

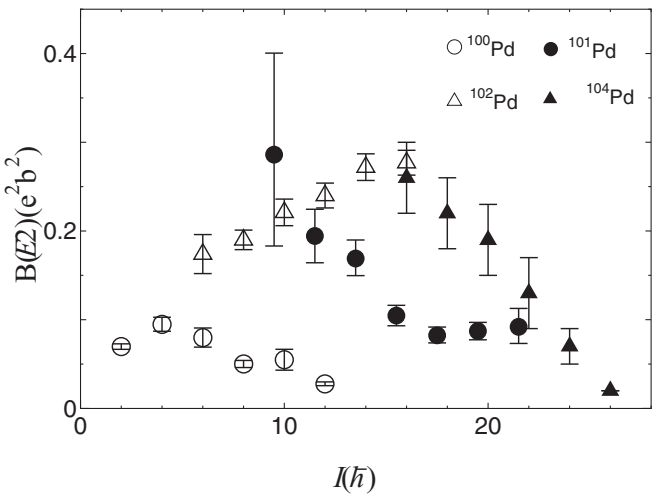

FIG. 3. Systematics of $B(E2)$ values as a function of spin values for the neighboring Pd nuclei around ^{101}Pd. The data on ^{100}Pd, ^{102}Pd, and ^{104}Pd are from Ref. [15], Ref. [16], and Ref. [7], respectively.

TABLE II. Configurations and parameters used for ^{106,108,110}Cd in the modified SCM calculation, in which the actual configuration changes smoothly from 1 to 2 at a certain spin region. The difference between the configurations 1 and 2 is with or without additional two-neutron alignment. Im, V_0, ω_0, $eQ_{\rm eff}$, α, and $\theta_{\rm c}$ are taken as free parameters to be fitted.

Nuclide	Configuration 1 Configuration 2	$J_\pi(n_\pi)$ Im(1/MeV)	$J_{\nu1}(n_{\nu1})$ $J_{\nu2}(n_{\nu2})$ V_0(MeV)	ω_0(MeV)	$eQ_{\rm eff}$(eb)	α	$\theta_{\rm c}(^\circ)$
^{106}Cd	$(\pi g_{9/2}^{-2}) \otimes (\nu h_{11/2}^2)$	9/2(1)	10(2)				
	$(\pi g_{9/2}^{-2}) \otimes (\nu h_{11/2}^2 g_{7/2}^2)$		14(4)[a]				
		10	0.32	0.25	1.0	20	77
^{108}Cd	$(\pi g_{9/2}^{-2}) \otimes (\nu h_{11/2}^2)$	9/2(1)	10(2)				
	$(\pi g_{9/2}^{-2}) \otimes (\nu h_{11/2}^2 g_{7/2}^2)$		12(4)[a]				
		10	0.30	0.25	1.0	10	64
^{110}Cd	$(\pi g_{9/2}^{-2}) \otimes (\nu h_{11/2})^2$	9/2(1)	10(2)[a]				
	$(\pi g_{9/2}^{-2}) \otimes (\nu h_{11/2}^4)$		14(4)[a]				
		10	0.35	0.26	1.15	3.3	35

[a]Assuming not fully aligned.

^{101}Pd nicely fall into the region between those for ^{100}Pd and ^{102}Pd (or ^{104}Pd).

The large $\mathrm{Im}^{(2)}/B(E2)$ values and the decreasing tendency of $B(E2)$ with the increasing spin shown in Table I indicates that the $\nu h_{11/2}$ band of ^{101}Pd has a required character as AMR at least in the lower part. However, because the $\mathrm{Im}^{(2)}/B(E2)$ values considerably fluctuate, the rising behavior of them along the band is barely seen on the average. Then, we proceed to a discussion in further support of our identification of the $\nu h_{11/2}$ band as AMR invoking a modified semiclassical particle-rotor model to include neutron alignments while the shears are closing. We briefly describe the model in Sec. III A. The predictions of the model are compared with the experimental data for several cases confirmed as AMR in Pd and Cd isotopes in the first part of Sec. III B to examine the applicability of the model. We finally address the discussion about whether the $\nu h_{11/2}$ band is really AMR or not by comparing the predictions of the model with the experimental data for ^{101}Pd.

A. A modified semiclassical particle-rotor model including neutron alignments

We extended the semiclassical particle-rotor model (SCM), which was originally devised by Macchiavelli *et al.* [17,18], to include AMR in Ref. [19]. That model was subsequently applied by Choudhury *et al.* [2] to ^{105}Cd to interpret higher-spin states of the negative-parity yrast band as AMR. As already mentioned in the introduction, relevant high-j orbitals for AMR in this region are $\pi g_{9/2}$ as a hole state and $\nu h_{11/2}$, $\nu g_{7/2}$, and $\nu d_{5/2}$ as particle states. Theoretically, Zhao *et al.* confirmed the "two-shears-like" mechanism for the AMR band in ^{105}Cd based on covariant density functional theory [10]. They also found the gradual alignment of the neutrons in the $g_{7/2}$ and $d_{5/2}$ orbitals along the band in addition to the almost constant alignment of the $h_{11/2}$ neutrons. Therefore we modified the SCM in our previous study to include neutron alignments to explore the possibility that the entire negative-parity yrast band can be described as AMR. The details of the model were described in Ref. [8].

According to our previous study, the total angular momentum $\vec{I}$ is generated from the proton-hole blades $\vec{J}_{\pi1}$ and $\vec{J}_{\pi2}$, the neutron blade $\vec{J}_\nu$, and the rotation $\vec{R}$ of the core. Here, we assume that each of $\vec{J}_{\pi1}$ and $\vec{J}_{\pi2}$ consists of n_π proton holes with mutually aligned angular momenta and that $\vec{J}_\nu$ consists of n_ν neutrons with rotation-aligned angular momenta. The energy formula is given as follows:

$$E(I,\theta) = \frac{(\vec{I}-\vec{J}_{\pi1}-\vec{J}_{\pi2}-\vec{J}_\nu)^2}{2\mathrm{Im}} + 2V_0 n_\pi n_\nu \left(\frac{3\cos^2\theta-1}{2}\right) - V_0 n_\pi^2 \left(\frac{3\cos^2 2\theta-3}{2}\right) + I\omega_0,$$

where Im, V_0, θ, and ω_0 stand for the moment of inertia of the core, the magnitude of the effective interaction for a particle-particle (or particle-hole) pair, the angle between the proton-hole blade and the neutron blade, and the band head frequency, respectively. The value of θ that minimizes the energy is obtained for any given value of I from the condition $(\frac{\partial E}{\partial\theta})_I = 0$, as follows:

$$I = (2J_\pi\cos\theta + J_\nu) + \frac{3\mathrm{Im}V_0}{J_\pi}\cos\theta\left(n_\pi n_\nu - 2n_\pi^2\cos 2\theta\right).$$

The value of ω is extracted from the canonical relation $\omega = \frac{\partial E}{\partial I}$ as follows:

$$\omega = \omega_0 + \frac{3V_0}{J_\pi}\cos\theta\left(n_\pi n_\nu - 2n_\pi^2\cos 2\theta\right).$$

However, at that time, the two configurations (the configurations 1 and 2 in Tables II and III) are considered separately. Here the model is further extended so the band property changes smoothly from configuration 1 to configuration 2. That is to say, we assume J_ν and n_ν gradually change from $J_{\nu1}$ and $n_{\nu1}$ to $J_{\nu2}$ and $n_{\nu2}$, respectively, while the shears are closing. A steplike function, such as

$$f(\theta) = \frac{1-\tanh(\alpha(\theta-\theta_{\rm c}))}{2},$$

can be used to implement this feature, where α and $\theta_{\rm c}$ represent the abruptness of the change and the critical angle at which the change occurs, respectively. Specifically, J_ν and n_ν are

TABLE III. Configurations and parameters used for ^{101,104}Pd in the modified SCM calculation, in which the actual configuration changes smoothly from 1 to 2 at a certain spin region. The difference between the configurations 1 and 2 is with or without additional two-neutron alignment. Im, V_0, ω_0, $eQ_{\rm eff}$, α, and θ_c are taken as free parameters to be fitted.

Nuclide	Configuration 1 Configuration 2	$J_\pi(n_\pi)$ $J_{\nu1}(n_{\nu1})$ $J_{\nu2}(n_{\nu2})$ Im(1/MeV)	V_0(MeV)	ω_0(MeV)	$eQ_{\rm eff}$(eb)	α	θ_c(°)
^{104}Pd	$(\pi g_{9/2}^{-4}) \otimes (\nu h_{11/2})^2$	6(2)	10(2)				
	$(\pi g_{9/2}^{-4}) \otimes (\nu h_{11/2}^2 g_{7/2}^2)$		11(4)[a]				
		14	0.18	0.27	1.29	14	50
^{101}Pd	$(\pi g_{9/2}^{-4}) \otimes (\nu h_{11/2})$	6(2)	11/2(1)				
	$(\pi g_{9/2}^{-4}) \otimes (\nu h_{11/2} g_{7/2}^2)$		23/2(3)				
		13	0.17	0.23	1.22	100	60

[a]Assuming not fully aligned.

expressed as follows:

$$J_\nu = J_{\nu1} + (J_{\nu2} - J_{\nu1}) f(\theta),$$
$$n_\nu = n_{\nu1} + (n_{\nu2} - n_{\nu1}) f(\theta).$$

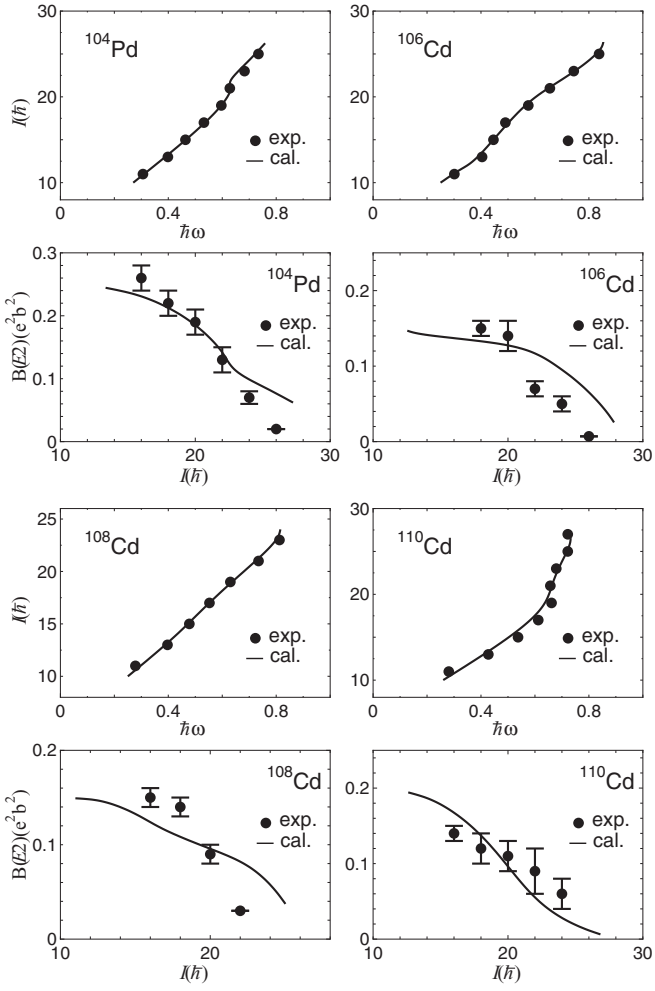

FIG. 4. The observed $I - \omega$ and $B(E2) - I$ behaviors for ^{104}Pd and ^{106,108,110}Cd are compared with the corresponding results obtained with the modified semiclassical model. The data on ^{104}Pd, ^{106}Cd, ^{108}Cd, and ^{110}Cd are from Ref. [7], Ref. [3], Ref. [4], and Ref. [6], respectively. The parameters used for the calculation are tabulated in Tables II and III.

The reduced transition probability within the band is given by

$$B(E2) = \frac{15}{32\pi}(eQ_{\rm eff})^2 \sin^4\theta,$$

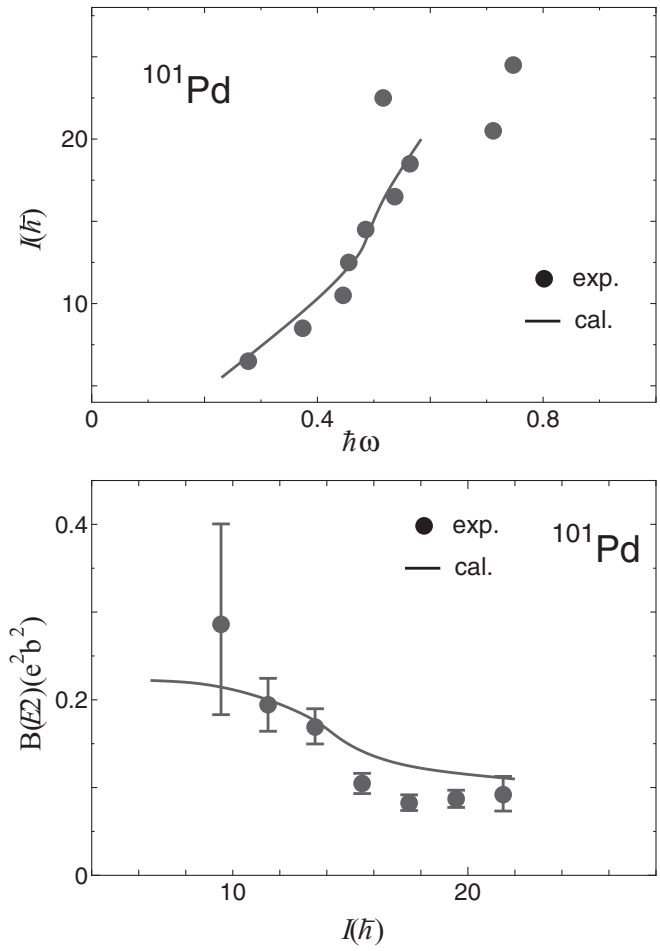

FIG. 5. The observed $I - \omega$ and $B(E2) - I$ behaviors for ^{101}Pd are compared with the corresponding results obtained from the modified semiclassical model. The parameters used for the calculation are tabulated in Table III.

according to Ref. [3], where $Q_{\rm eff}$ is the effective quadrupole moment of the antimagnetic rotor which mainly comes from protons.

B. Comparison of the model calculation with the experimental result

Plots of spin against $\hbar\omega$ and $B(E2)$ against spin obtained from the semiclassical model described above can be compared with the corresponding plots for the Cd and Pd isotopes studied experimentally, as shown in Fig. 4. Because Cd(Pd) isotopes include two (four) proton holes in the $Z = 50$ shell, $\pi g_{9/2}^{-2}(\pi g_{9/2}^{-4})$ is taken as the proton configuration. Rotational alignments of $\nu g_{7/2}^2$ or $\nu h_{11/2}^2$ are included while we consider the neutron configuration to describe the entire band. Specific configurations and parameters used in the model calculation are shown in Tables II and III, where Im, V_0, ω_0, α, and $\theta_{\rm c}$ are regarded as free parameters to be fitted for each band. It is important to note that good agreements are obtained for both plots of $I - \hbar\omega$ and $B(E2)-I$ as seen in the figure within a reasonable range of parameters for the cases considered here.

Encouraged by this result, we apply the same model to the $\nu h_{11/2}$ band in ^{101}Pd whose lifetimes have been measured in the present experiment. Plots of $I - \hbar\omega$ and $B(E2)-I$ obtained from the experimental results are compared with the corresponding plots of the model calculation in Fig. 5. The configurations and parameters used in the model calculations are listed in Table III. Clearly, both $I - \hbar\omega$ and $B(E2)-I$ behaviors are described somewhat well in a consistent way except for the uppermost three states, as for which the irregularity seen in the plot of $I - \hbar\omega$ indicates that a kind of structural change might occur. Therefore, it is reasonable to conclude that the lower part of the $\nu h_{11/2}$ band in ^{101}Pd is another example of the AMR band in this region.

IV. SUMMARY

We presented the result of lifetime measurements for the $\nu h_{11/2}$ band in ^{101}Pd, which were obtained through the line-shape analysis of γ rays from the reaction ^{68}Zn(^{37}Cl, 1p3n)^{101}Pd. We observed the large $\mathcal{I}^{(2)}/B(E2)$ values and the decreasing tendency of $B(E2)$ with the increasing spin at the lower part of the band. These characters are reproduced somewhat well by a modified semiclassical particle-rotor model in a consistent way for other AMR bands in Cd and Pd isotopes. Therefore we can conclude that the lower part of the $\nu h_{11/2}$ band in ^{101}Pd is another example of AMR in this region.

ACKNOWLEDGMENTS

We thank the team operating the JAEA tandem accelerator for providing the heavy-ion beams used in the experiment.

[1] S. Frauendorf, Rev. Mod. Phys. **73**, 463 (2001).
[2] D. Choudhury, A. K. Jain, M. Patial, N. Gupta, P. Arumugam, A. Dhal, R. K. Sinha, L. Chaturvedi, P. K. Joshi, T. Trivedi *et al.*, Phys. Rev. C **82**, 061308(R) (2010).
[3] A. J. Simons, R. Wadsworth, D. G. Jenkins, R. M. Clark, M. Cromaz, M. A. Deleplanque, R. M. Diamond, P. Fallon, G. J. Lane, I. Y. Lee *et al.*, Phys. Rev. Lett. **91**, 162501 (2003).
[4] A. J. Simons, R. Wadsworth, D. G. Jenkins, R. M. Clark, M. Cromaz, M. A. Deleplanque, R. M. Diamond, P. Fallon, G. J. Lane, I. Y. Lee *et al.*, Phys. Rev. C **72**, 024318 (2005).
[5] P. Datta, S. Chattopadhyay, S. Bhattacharya, T. K. Ghosh, A. Goswami, S. Pal, M. S. Sarkar, H. C. Jain, P. K. Joshi, R. K. Bhowmik *et al.*, Phys. Rev. C **71**, 041305(R) (2005).
[6] S. Roy, S. Chattopadhyay, P. Datta, S. Pal, S. Bhattacharya, R. K. Bhowmik, A. Goswami, H. C. Jain, R. Kumar, S. Muralithar *et al.*, Phys. Lett. B **694**, 322 (2011).
[7] N. Rather, S. Roy, P. Datta, S. Chattopadhyay, A. Goswami, S. Nag, R. Palit, S. Pal, S. Saha, J. Sethi *et al.*, Phys. Rev. C **89**, 061303(R) (2014).
[8] M. Sugawara, T. Hayakawa, M. Oshima, Y. Toh, A. Osa, M. Matsuda, T. Shizuma, Y. Hatsukawa, H. Kusakari, T. Morikawa *et al.*, Phys. Rev. C **86**, 034326 (2012).
[9] A. V. Afanasjev, D. B. Fossan, G. J. Lane, and I. Ragnarsson, Phys. Rep. **322**, 1 (1999).
[10] P. W. Zhao, J. Peng, H. Z. Liang, P. Ring, and J. Meng, Phys. Rev. C **85**, 054310 (2012).
[11] K. Furuno, M. Oshima, T. Komatsubara, K. Furutaka, T. Hayakawa, M. Kidera, Y. Hatsukawa, M. Matsuda, S. Mitarai, T. Shizuma *et al.*, Nucl. Instrum. Methods Phys. Res. A **421**, 211 (1999).
[12] J. C. Wells and N. R. Johnson, Oak Ridge National Laboratory Report No. ORNL-6689 (ORNL, Oak Ridge, 1991).
[13] L. C. Northcliffe and R. F. Schilling, At. Data Nucl. Data Tables **7**, 233 (1970).
[14] F. James and M. Roos, Comput. Phys. Commun. **10**, 343 (1975).
[15] D. Radeck, A. Blazhev, M. Albers, C. Bernards, A. Dewald, C. Fransen, M. Heidemann, J. Jolie, B. Melon, D. Mücher *et al.*, Phys. Rev. C **80**, 044331 (2009).
[16] A. D. Ayangeakaa, U. Garg, M. A. Caprio, M. P. Carpenter, S. S. Ghugre, R. V. Janssens, F. G. Kondev, J. T. Matta, S. Mukhopadhyay, D. Patel *et al.*, Phys. Rev. Lett. **110**, 102501 (2013).
[17] A. O. Macchiavelli, R. M. Clark, M. A. Deleplanque, R. M. Diamond, P. Fallon, I. Y. Lee, F. S. Stephens, and K. Vetter, Phys. Lett. B **450**, 1 (1999).
[18] R. M. Clark and A. O. Macchiavelli, Annu. Rev. Nucl. Part. Sci. **50**, 1 (2000).
[19] M. Sugawara, Y. Toh, M. Oshima, M. Koizumi, A. Osa, A. Kimura, Y. Hatsukawa, J. Goto, H. Kusakari, T. Morikawa *et al.*, Phys. Rev. C **79**, 064321 (2009).